IEEE Access
Multidisciplinary | Rapid Review | Open Access Journal

IEEE POWER & ENERGY SOCIETY SECTION

Received 24 September 2024, accepted 11 November 2024, date of publication 13 November 2024,
date of current version 21 November 2024.

Digital Object Identifier 10.1109/ACCESS.2024.3497669

RESEARCH ARTICLE

Impact of Synchronous Condensers on Small-Signal Stability of Offshore Wind Power Plants

SULAV GHIMIRE[1,2], (Graduate Student Member, IEEE), KANAKESH VATTA KKUNI[1], (Member, IEEE), EMERSON D. GUEST[1], KIM H. JENSEN[1], AND GUANGYA YANG[2], (Senior Member, IEEE)

[1]Siemens Gamesa Renewable Energy A/S, 7330 Brande, Denmark
[2]Department of Wind and Energy Systems, Technical University of Denmark, 2800 Kongens Lyngby, Denmark

Corresponding author: Sulav Ghimire (sulav.ghimire@siemensgamesa.com)

The work of Sulav Ghimire was supported by Innovation Fund Denmark under Project 0153-00256B.

ABSTRACT Grid-forming (GFM) converter control technology and synchronous condensers (SCs) have both been reported to improve the overall stability of a power system. GFM technology is being considered for offshore wind power plants (OF WPPs) due to their stabilising effect, and SCs are being integrated into OF WPPs as they increase the short circuit level of the system. This paper investigates the effect of SCs on the small-signal stability of an OF WPP with different converter control strategies, namely grid-following (GFL) and grid-forming (GFM). Primarily, the effect of SCs can be two-fold: (1) overall stability enhancement of the WPP by providing reactive power support, and (2) contribution to the effective short circuit ratio (SCR) of the WPP by fault current support. Therefore, this paper focuses on studies concerning these effects on an aggregated model of a WPP connected to the grid. This paper also tries to compare the stabilising effects of GFM converters and SCs by comparing the small-signal stability of the test system with GFL control and SC and with GFM control. To that end, a state-space model of the test system is developed for small-signal stability assessment and the SC's effect on its stability. In addition, a mathematical explanation of SCR enhancement with an SC is provided and is verified against the fault MVA calculations done on time-domain simulation models.

INDEX TERMS Grid-following, grid-forming, offshore wind power plants, stability, synchronous condensers, weak grids.

I. INTRODUCTION

Modern offshore wind power plants (OF WPPs) are connected to the grid via long sea cables characterised by their low X/R ratio and low short circuit ratio (SCR) [1]. WPPs connected to weak grids need to supply larger reactive power to supply the same active power than WPPs connected to stronger grids (ref. Appendix C, Figure 10). The low SCR and low inertia of the existing power grid imply lower fault current contribution from the grid; thus, the grid connection is termed a weak grid. Small-signal stability studies have shown that low SCR weak-grid connections can introduce an open-loop zero in the right half plane of the system, leading to oscillations that are poorly damped or undamped [2]. The low X/R ratio also enhances the P-V and Q-f coupling, which would otherwise be negligible in a grid with a high X/R ratio since the resistance is negligible compared to the reactance [1]. In a weakly connected OF WPP, a reactive power support device at the point of common coupling (PCC) helps to supply higher fault currents [3], provide better reactive power support, and aid in post-fault voltage recovery [4]. This further aids the WPP in operating smoothly during steady state as well as during fault-ride through (FRT).

The associate editor coordinating the review of this manuscript and approving it for publication was Ning Kang.

Synchronous condensers (SCs) have been known to stabilise power systems by providing damping to generator power swings and reactive power injection [5]. Stability enhancement by compensation devices such as SCs, SVCs, and STATCOMs spans localised parts of power systems such as WPPs and large-scale national and regional interconnected power systems. Energinet, the Danish transmission system operator (TSO), also believes synchronous condensers can ensure power system stability [6] and also provide ancillary services [7]. It is understood that improving voltage regulation and reactive power compensation is an important factor for stable power system operation [8]. The Nordic TSOs agree that adding rotating masses, such as SCs, can help tackle the low-inertia issue in large-scale power systems [9].

There have been some examples of stability enhancement of OF WPPs with the help of a reactive power support device such as STATCOM, static var compensator (SVC), or SC. e.g., A WPP connected to Texas' ERCOT grid experienced low-frequency oscillations due to weak-grid connections, which were subsequently seen to be damped by SVCs and SCs [10]. The Granite substation in Vermont-US also used an SC to enhance the stability and reactive power capability [11]. The academic literature also includes works on applying SCs for frequency support and reactive power support services. e.g., [12] show that SCs can also improve the frequency. However, [13] claims that a power electronics converter-based frequency support system can provide better frequency support than the SCs provided it is connected to a generation source. A real-life application of SCs for frequency stability includes the Talega substation in California, where the SC was applied to support the power system voltage and frequency stability [14]. The authors of [14] also compare the features of SCs, static var compensators (SVCs), and STATCOMs, which shows that an SC has an overall superior performance to SVC and STATCOM as it provides short-circuit power contribution, dynamic reactive power support, voltage recovery after a fault, inertial response and frequency support, and exhibits resilience to harmonics and over/under-voltage capacities. SCs can also help control the wind-farm transient voltage under communication failure using an 'online sequential extreme learning machine' based voltage prediction method [4].

In a comparative analysis between STATCOM and SCs for wind-farm applications, results show that SCs can improve the stability of a WPP with grid-following (GFL) type-IV wind turbine generators (WTGs) connected to a weak grid; it is seen to improve the system stability even when it is not injecting any reactive power [15]. On the other hand, a STATCOM improves the stability of a WPP only by injecting reactive power. Grid-forming (GFM) converter control technology is also reported to have increased the system stability for weakly connected systems [16] and is the subject of a vast amount of ongoing research.

Previous work supports using SCs in modern power systems as they increase the short-circuit performance, overload capabilities, and inertial support and facilitate the integration of more inverter-based resources [17]. Weak-grid applications of SCs have been proposed along with battery energy storage systems (BESS) in [18], where the SC significantly improved overload capacity while retaining the fast response of a converter-integrated BESS. A similar application could be found for OF WPPs with weak-grid connections. Although SCs can enhance the protection performance of a type-IV WPP, it has been seen that the converter control strategy also highly affects the overall performance of the WPP [19].

Optimal allocation of SCs in a simplified Danish grid model is provided in [20], where the authors state that the use of SCs improves the SCR of the system. However, a mathematical quantification for SCR enhancement is not presented. Additionally, they follow the approach of converting the Thevenin equivalent model of SC to the Norton equivalent model. In contrast, our work uses the Thevenin equivalent for the SC model as it aids in deriving the expression for the equivalent SCR of the system.

Research works on optimal placement of SCs in wind-dominated power grids are presented in [21], where the authors show the SCR improvement in the power system with the help of synchronous condensers. However, the work primarily focuses on the optimal allocation of SCs to minimise the total cost, and insights on small-signal stability or mathematical re-formulation of the improved SCR are lacking. Our work, although not focussed on the optimal placement of SCs due to the scope of the research, succeeds in mathematically quantifying the SCR enhancement by SCs and demonstrates the improvement of small-signal stability.

A comparison of SCs with STATCOMs in a doubly-fed induction generator (DFIG) and permanent magnet synchronous generator (PMSG)-based wind farms is presented in [22] with some insights on small-signal stability; however, the focus is on sub/super-synchronous oscillations. Further, the small-signal stability studies presented in [22] are limited by eigenvalue trajectories for cases with and without SCs at different wind speeds. In contrast, our work presents eigenvalue plots for various operating points for different grid SCR values, as well as WTG power and voltage controller step responses. Further, a participation factor analysis of one unstable pole pair is presented in the Appendix for reference.

Previous works discussed herewith adopted time-domain approaches to study the reactive power and frequency support aspect of SCs. Some studies related to transient stability, dynamic voltage stability, small-signal stability studies, and sub/super-synchronous oscillation studies are also seen in the recently published research. However, the existing literature does not present detailed small-signal stability studies, including eigenvalues and controller step responses. Further, as discussed above, although some works indicate the SCR enhancement of an existing system via SCs, they do not include an expression for the equivalent SCR enhancement

and their verification against SCR values obtained from fault simulations. Further, no comparative analysis could be seen in the existing literature which addresses the topic of SCs on OF WPPs and how SCs impact the stability of OF WPPs with different converter control technologies, namely GFM and GFL. Our paper fills the identified research gaps: the small-signal stability effect of SCs on an OF WPP, SCR enhancement, and its performance for WPP with GFM and GFL technologies.

The key contributions of this paper are summarised as:

- Small-signal stability of an OF WPP with the addition of SCs and cases for GFM and GFL technologies in the WTGs.
- Quantification of SCR enhancement of an OF WPP with the addition of SCs.

The paper layout is as follows: Section II describes the system setup, its modelling (time-domain and frequency-domain small-signal model development), and adopted methodology (small-signal stability analysis and time-domain fault simulation). Section III describes the mathematical formulation of the equivalent SCR enhancement due to the effect of the SC. Section IV provides the results obtained and a detailed analysis and discussion of the results. Finally, Section V summarises the findings and provides a conclusion based on the studies presented in the paper.

II. SYSTEM SETUP AND MODELLING

For various simulation-based studies of a power system, including an offshore wind power plant, various modelling practices could be adopted based on the requirement. Whenever an overall view of system static and dynamic operation and stability analysis is required, full-order nonlinear dynamical models in EMT domains, reduced-order RMS models, and linearised small-signal models are used in unison. Various modelling practices offer different fidelity and have advantages and drawbacks over the other modelling practices [23]. For our study, a small-signal model is crucial and more relevant for stability studies over a wide range of operating points, while time-domain simulations based on higher-order models were necessary to verify SCR enhancement with SCs. Thus, the primary modelling practice followed in this paper is small-signal modelling (Section II-B), with some use of detailed time-domain models (Section IV-C).

The system under study consists of an aggregated WPP connected to a grid through an array cable and a transformer, as shown in figure 1. The array cable has an impedance Z_a, and the grid has an impedance $Z_g = R_g + jX_g$. An SC with sub-transient reactance $Z_{sc} = jX''_{sc}$ is connected at the PCC.

All parameters are represented in pu; differential and algebraic variables are represented in small-signal pu when denoted by a lowercase letter and are in large-signal SI units when denoted by an uppercase letter.

A. GRID AND SYNCHRONOUS CONDENSER MODEL

The grid is modelled as a Thevenin equivalent source, i.e., an ideal voltage source ($\tilde{V}_g = 1\angle 0°$) behind an impedance Z_g. The load-flow behaviour of a grid thus modelled would be that of a $P - \delta$ bus. The mathematical model of the grid used to build its time-domain model can be written as:

$$\tilde{V}_g = 1\angle 0°, \tag{1}$$

$$\tilde{I}_g = \frac{\tilde{V}_g - \tilde{V}_{pcc}}{R_g + jX_g}, \tag{2}$$

$$S_g = P_g + jQ_g = \tilde{V}_g \tilde{I}_g^*, \tag{3}$$

where, $\tilde{V}_g$ is the grid voltage, $\tilde{V}_{pcc}$ is the PCC voltage, $Z_g = R_g + jX_g$ is the grid impedance, $\tilde{I}_g$ is the current flowing from the grid towards PCC, and $S_g = P_g + jQ_g$ is the grid apparent power whose real part P_g is the active power and imaginary part Q_g is the reactive power. The $(\tilde{\cdot})$ above the variables indicate that they are phasor variables.

The state equation relating to the small-signal model of the grid is,

$$L_g \dot{i}_{g,dq} = -R_g i_{dq}^{(g)} + jX_g i_{dq}^{(g)} + v_{dq}^{(g)} - v_{dq}^{(pcc)}. \tag{4}$$

Similar to the grid, an SC is modelled as a Thevenin equivalent model, i.e., an ideal voltage source behind the sub-transient reactance. This modelling approach is valid for small-signal stability and fault studies since during the fault cases and fast transients, the sub-transient reactance of the SC becomes active [24], [25] and has also been adopted in the academic literature [20]. Energinet also follows a similar modelling approach for some of their studies [26].

SC controls are bypassed for this study as their responses are very slow and only impact the low-frequency ranges. The load-flow behaviour of the SC is that of a $P - V$ bus with a small active power loss $|P| \ll 1$ pu. The mathematical model of the SC is thus given as,

$$\tilde{V}_{sc} = 1\angle \varphi_{sc}, \tag{5}$$

$$\tilde{I}_{sc} = \frac{\tilde{V}_{sc} - \tilde{V}_{pcc}}{jX''_{sc} + R_{tr} + jX_{tr}}, \tag{6}$$

$$S_{sc} = P_{sc} + jQ_{sc} = \tilde{V}_{sc} \tilde{I}_{sc}^* \approx Q_{sc}, \tag{7}$$

where $\tilde{V}_{sc}$ is the SC voltage, $\tilde{I}_{sc}$ the current, X''_{sc} the sub-transient reactance, and Q_{sc} is its reactive power contribution. The transformer is modelled inside the abovementioned equations, and $R_{tr} + jX_{tr}$ represents the transformer impedance. The transformer used in this paper is a $Y - Y$ transformer; thus, no phase-shift adjustment is necessary.

Now, the state equation relating to the small-signal model of the SC is written as,

$$\frac{X''_{sc}}{\omega_0} \dot{i}_{dq}^{(sc)} = R_{tr} i_{dq}^{(sc)} + j(X''_{sc} + X_{tr}) i_{dq}^{(sc)} + v_{dq}^{(sc)} - v_{dq}^{(pcc)}. \tag{8}$$

The equivalent circuit of the power grid and SC thus modelled are shown in Figure 2.

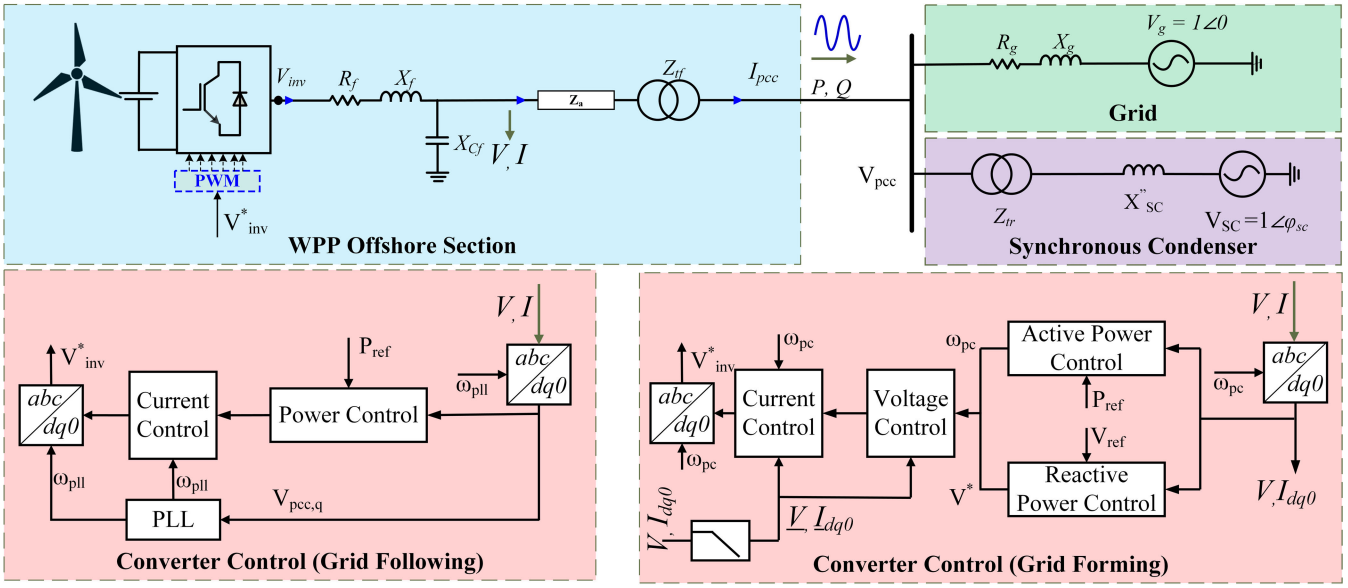

FIGURE 1. Aggregated WPP layout with an SC connected at PCC.

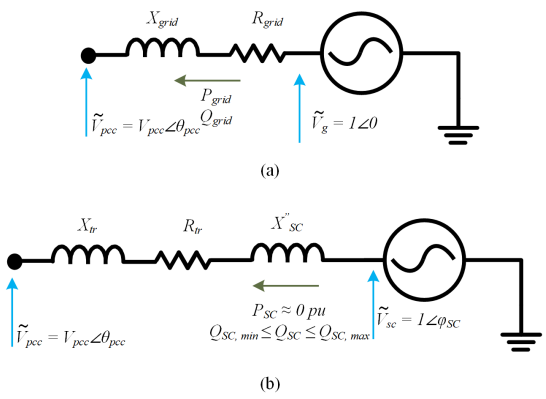

FIGURE 2. Thevenin equivalent models for (a) power grid and (b) SC and transformer used in the study.

B. WPP CONVERTER MODELS

Two different control methods for the WPP converters are selected for the studies, namely grid-following (GFL) control and grid-forming (GFM) control, as shown in Figure 1. Although the detailed modelling of these controls is not included, an averaged state-space model is presented in this paper.

1) GRID-FOLLOWING CONTROL (GFL)

The converter control model is derived from [27]. The grid following control includes a phase-locked loop (PLL) as the synchronizing unit which is modelled as:

$$\dot{\theta}_{pll} = \omega_0 + \left(K_p^{(pll)} + \frac{K_i^{(pll)}}{s}\right) v_q, \tag{9}$$

where, θ_{pll} is the PLL phase angle, $\omega_0 = 2\pi f_0$ is the nominal angular frequency, v_q is the quadrature axis voltage which servers as an input to the PLL, and $K_p^{(pll)}$ and $K_i^{(pll)}$ are the PLL proportional and integral gains respectively.

The power controller generates a current reference signal for the current controller which is given as:

$$i_d^* = (p^* - p_{pc}) \left(K_p^{(pc)} + \frac{1}{s} K_i^{(pc)}\right), \tag{10}$$

$$i_q^* = 0, \tag{11}$$

where, $p_{pc} = v_d i_d + v_q i_q$, and $q_{pc} = v_q i_d - v_d i_q$ are the small-signal active and reactive powers of the converter in pu, $K_p^{(pc)}$ and $K_i^{(pc)}$ are the PI-gains of the power controller, and v_{dq} and i_{dq} represent the voltage and current at the measurement points.

The current controller is implemented as a PI-controller, and the control method is given as:

$$G_{pic}(s) = K_p^{(cc)} + \frac{K_i^{(cc)}}{s}, \tag{12}$$

$$v_{idq}^* = v_{dq}^{(pcc)} + G_{pic}(s)(i_{dq}^* - i_{dq}) + jX_f i_{dq}. \tag{13}$$

Here, v_{idq}^* are the inverter reference voltage signals, which, when transformed into the $abc-$frame, are fed into the PWM block. $G_{pic}(s)$ is the PI-controller transfer function implemented for current control.

The linearised state-space equations of the GFL converter can be summarised as follows:

$$\dot{\theta}_{pll} = \omega_0 + K_p^{(pll)} v_q + K_i^{(pll)} \mathcal{S}, \tag{14}$$

$$\dot{\mathcal{S}} = v_q, \tag{15}$$

$$\dot{\gamma} = -\frac{K_i^{(pc)}}{K_p^{(pc)}} \gamma + \frac{1}{K_p^{(pc)}} i_d^*, \tag{16}$$

$$\dot{\mathcal{O}}_{dq} = i_{dq}^* - i_{dq}, \tag{17}$$

where, θ_{pll} is the PLL phase angle, $\omega_0 = 2\pi f_0$ is the nominal angular frequency, and $K_p^{(pll)}$ and $K_i^{(pll)}$ are the PLL proportional and integral gains respectively. γ is the power controller state given as the integral of small-signal power mismatch, i.e. $\dot{\gamma} = p^* - p_{pc}$. p_{pc} and q_{pc} are the small-signal active and reactive powers of the converter, v_{dq} and i_{dq} represent the voltage and current at the measurement points, $\mathcal{S}$ is a PLL-state which is given as $\dot{\mathcal{S}} = v_q$, and $\mathcal{O}_{dq}$ are the current controller states. Now, the converter voltage reference signals can be written as:

$$v_{idq}^* = v_{dq}^{(pcc)} + K_p^{(cc)}(i_{dq}^* - i_{dq}) + K_i^{(cc)}\mathcal{O}_{dq}. \tag{18}$$

2) GRID-FORMING (GFM) CONTROL

A virtual synchronous machine (VSM) based GFM control is implemented. The GFM converter control used in this paper is adapted from [28].

The power controller dynamics of the GFM converter control method are given as:

$$\theta_{pc} = \int \left[\omega_0 + \frac{1}{Js + D_p}(p^* - p_{pc})\right] dt, \tag{19}$$

$$v_d^* = v_n - K_q(q^* - q_{pc}), \tag{20}$$

$$v_q^* = 0. \tag{21}$$

Here, J is the VSM inertia constant, D_p is the VSM damping term, and θ_{pc} is the angle given by the power controller.

The voltage control loop dynamics is implemented as a PI controller and is governed by the following equations:

$$G_{piv}(s) = K_p^{(vc)} + \frac{K_i^{(vc)}}{s}, \tag{22}$$

$$i_{dq}^* = i_{dq}^{(pcc)} + G_{piv}(s)(v_{dq}^* - v_{dq}) + \frac{jv_{dq}}{X_{C_f}}. \tag{23}$$

Here, $G_{piv}(s)$ is the voltage controller transfer function. These current reference signals i_{dq} are sent to the current controller, which compares it with the current measurement. The current controller is also a PI-based controller, and its dynamics are given as:

$$G_{pic}(s) = K_p^{(cc)} + \frac{K_i^{(cc)}}{s}, \tag{24}$$

$$v_{idq}^* = v_{dq}^{(pcc)} + G_{pic}(s)(i_{dq}^* - i_{dq}) + jX_f i_{dq}. \tag{25}$$

The linearised state-space equations of the GFM converter are given as:

$$\dot{\theta}_{pc} = \omega_{pc} \tag{26}$$

$$J\dot{\omega}_{pc} = p^* - p_{pc} - D_p\omega_{pc} \tag{27}$$

$$\dot{\mathcal{M}}_{dq} = v_{dq}^* - v_{dq} \tag{28}$$

$$\dot{\mathcal{O}}_{dq} = i_{dq}^* - i_{dq} \tag{29}$$

where, and $\mathcal{M}_{dq}$ and $\mathcal{O}_{dq}$ are the voltage controller and current controller states respectively. The voltage controller and current controller output equations are written as follows.

$$i_{dq}^* = i_{dq}^{(pcc)} + G_{piv}(s)(v_{dq}^* - v_{dq}) + \frac{jv_{dq}}{X_{C_f}}, \tag{30}$$

$$v_{idq}^* = v_{dq}^{(pcc)} + G_{pic}(s)(i_{dq}^* - i_{dq}) + jX_f i_{dq}, \tag{31}$$

where $G_{piv}(s) = K_{pv} + \frac{1}{s}K_{iv}$ and $G_{pic}(s) = K_{pc} + \frac{1}{s}K_{ic}$ denote the PI-controller implemented in the voltage and current control loops respectively.

The PWM block is modelled as a delay of T_{pwm} given as follows:

$$G_{PWM}(s) = e^{-sT_{pwm}}. \tag{32}$$

A Pade approximation of this delay is performed with a sampling time of T_s is given as:

$$G_{PWM}(s) \approx \frac{1 - \frac{T_s}{2}s}{1 + \frac{T_s}{2}s}. \tag{33}$$

3) FILTER AND ARRAY CABLE MODEL

Based on Kirchhoff's voltage and current laws, the state-space model of the converter's filter and array cable can be written as a set of differential-algebraic equations and are given as:

$$L_f\dot{i}_{f,dq} = -R_f i_{f,dq} + jX_f i_{f,dq} - v_{c,dq} + v_{dq}^{(inv)}, \tag{34}$$

$$C_f\dot{v}_{c,dq} = i_{f,dq} + j\omega_0 C_f v_{c,dq} - i_{a,dq}, \tag{35}$$

$$L_{a,tf}\dot{i}_{a,dq} = v_{c,dq} - R_{a,tf} i_{a,dq} + jX_{a,tf} i_{a,dq} - v_{dq}^{(pcc)}. \tag{36}$$

Here, R_f, L_f, C_f are the filter resistance, inductance, and capacitance, L_a, R_a are the array cable inductance and resistance, and L_{tf}, R_{tf} are the transformer inductance and resistance respectively. Also, $R_{a,tf}$ and $L_{a,tf}$ are given as $R_a + R_{tf}$ and $L_a + L_{tf}$ respectively and $X_{a,tf} = \omega_0 L_{a,tf}$.

III. SCR ENHANCEMENT

The short circuit ratio of a WPP at any given point is given as the ratio of the grid's fault MVA contribution to the WPP-rated power.

$$\text{i.e. } SCR = \frac{S_{g,f}}{S_{WPP}}, \tag{37}$$

where, $S_{g,f}$ is the grid fault contribution and S_{WPP} is the WPP's rated apparent power.

Assuming 1 pu voltage being maintained at the grid during the fault, and $S_{WPP} = 1$ pu, we can rewrite the system SCR as:

$$SCR = \frac{V_{g,pu}^2/|Z_{g,pu}|}{1\ pu} = \frac{1}{|Z_{g,pu}|}. \tag{38}$$

An SC behaves as a voltage source behind its sub-transient reactance under conditions valid for small-signal studies [24], [25]. Assuming 1 pu voltage behind the sub-transient reactance, an SC can be aggregated with the grid to observe an effective rise in the equivalent short circuit ratio (ESCR) at PCC.

From (38), we know that the SCR of a WPP at PCC can be given as the reciprocal of the pu grid impedance at 1 pu grid voltage. In a WPP, the base SCR value at WT MV terminals without considering the SC is written as:

$$\text{i.e. } SCR_o = \frac{1}{Z_{g,pu} + Z_{a,tf,pu}}. \tag{39}$$

Here, the impedance $Z_{g,pu} := |Z_{g,pu}|$ and $Z_{a,tf,pu} := |Z_{a,pu} + Z_{tf,pu}|$ are the absolute value of the sum of the respective impedances. Henceforth, unless otherwise stated, the same convention is followed for all other impedances.

Considering the stabilising effect and fault MVA contribution of an SC on SCR evaluation, we can view the grid and SC pair from PCC as two parallel voltage sources. Thus, we can write for the pu impedance seen at PCC as

$$Z_{PCC,pu} = \frac{Z_{g,pu} \cdot Z_{sc,pu}}{Z_{g,pu} + Z_{sc,pu}} < \min(Z_{g,pu}, Z_{sc,pu}). \tag{40}$$

The effective SCR at WT MV terminal can now be written as:

$$SCR_{sc} = \frac{1}{Z_{PCC,pu} + Z_{a,tf,pu}}. \tag{41}$$

Here, since $Z_{PCC,pu} < Z_{g,pu}$, it implies that $\text{SCR}_{sc} > SCR_o$. Thus, effective SCR at the WT MV terminal, considering the SC, is higher than without the SC. The physical interpretation of this is that the short-circuit MVA contribution of the SC increases the overall fault MVA of the system, thus increasing the effective SCR.

We can now write for this new effective SCR, including the effect of the SC as:

$$SCR_{sc} = \frac{Z_{g,pu} + Z_{sc,pu}}{Z_{g,pu} \cdot Z_{sc,pu} + Z_{a,tf,pu}(Z_{g,pu} + Z_{sc,pu})}. \tag{42}$$

The SCR enhancement quantification provided in equation (42) is verified with SCR values calculated from time-domain fault simulations, including the effect of SC in the system.

IV. RESULTS AND DISCUSSION

The small-signal and time-domain simulation models developed for the test system presented in Figure 1 are subjected to different tests. Frequency domain studies involving the step-responses of power and voltage controllers of the converter controls are presented in this section, where small-signal stability information is observed, e.g. controller reference tracking, oscillations and damping based on step responses, and stability/instability based on eigenvalue plots. The WPP's SCR is calculated before and after the addition of the SC based on (a) fault simulations and (b) theoretical calculations based on the method described in Section III, and are presented in this section.

Different grid conditions and operating points are chosen for the frequency-domain analysis and studies. IEEE guidelines [29] classify system strength in terms of SCR: a very weak grid has very low SCR$<$ 2, a weak grid has $2 < SCR \leq 3$, and a strong grid has SCR$\geq$ 3. An OF WPP's SCR is measured from the turbine MV terminals. SCR has a critical effect on system stability, and the study of extreme SCR cases becomes necessary for such systems. In order to study the effect of SCs on the stability of a WPP for different grid strengths, three grid strength cases are chosen and summarised in Table 1 in terms of grid SCR and X/R.

TABLE 1. Grid cases in terms of SCR at WT MV terminal.

Grid Case	Base-Case SCR	X/R Ratio
Weak Grid	1.6	5
Normal Grid	3.2	14.8
Strong Grid	4.12	14.8

The grid parameters, namely grid resistance and reactance, are defined based on the SCR and X/R values since we perform the simulations and calculations for different grid strength levels. From equation (38), we can obtain the magnitude of the grid impedance $|Z_{g,pu}|$ for different SCR values in Table 1 as $|Z_{g,pu}| = 1/SCR$. Further, the respective X/R ratios are provided in Table 1, which could be used to calculate the grid impedance in terms of resistance and reactance as,

$$Z_{g,pu} = \frac{1}{SCR}(\cos\varrho + j\sin\varrho) \tag{43}$$

where $\varrho = \tan^{-1}(X/R)$ is the impedance angle.

A. CONVERTER CONTROL STEP RESPONSES

The step responses of the power and voltage controllers for each of these cases are presented in Figure 3 (weak grid), Figure 4 (normal grid), and Figure 5 (strong grid). System references/operating points for the presented step responses are grid reference voltage $V_g^* = 1$ pu, turbine reference voltage $V_{turb}^* = 1$ pu, and turbine reference power $P_{turb}^* = 1$ pu, respectively.

1) WEAK GRID CASE

The step responses in Figure 3 show that for the provided system, i.e. a weakly connected WPP with GFL control, adding an SC at PCC can stabilize the previously unstable system. Furthermore, although instability is not observed in the response of GFM control, the inset in the power controller step responses shows that the initial oscillations are damped with the addition of an SC.

For the unstable case observed herewith, we perform a participation factor (PF) analysis to gain a deeper insight into the stability mechanism, especially to find out the states participating in such unstable modes. Since our approach does not involve system control parameters tuning, the PF analysis result is only included in Appendix B in Table 7 for general reference.

2) NORMAL GRID CASE

For the given operating point in a normal grid-connected GFM WPP, Figure 4 shows that no instability issue is seen

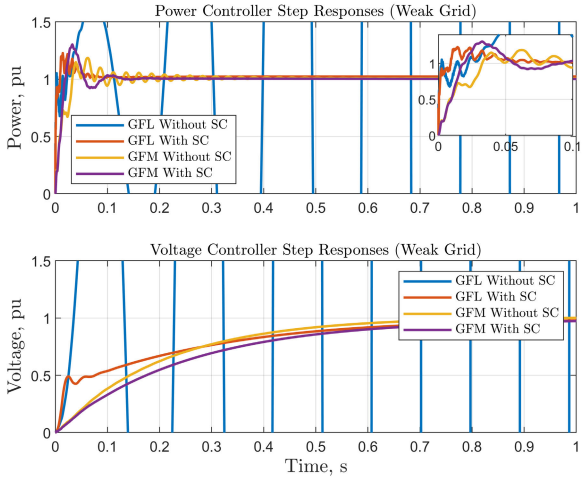

FIGURE 3. Power and voltage controller step response of GFL and GFM converters in a weakly connected WPP with and without an SC.

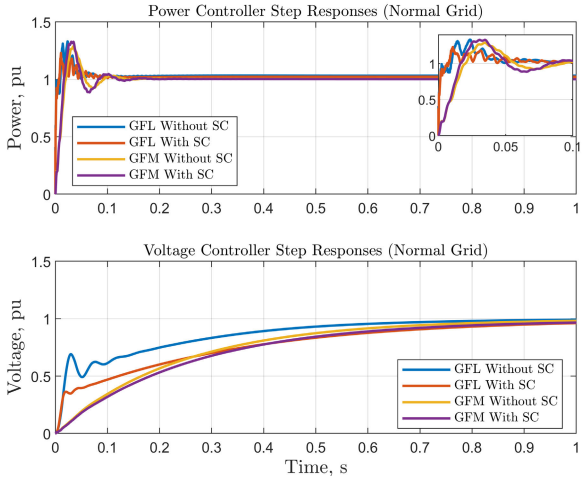

FIGURE 4. Power and voltage controller step response of GFL and GFM converters in a normal-grid connected WPP with and without an SC.

in the base case, and there is no significant effect on power and voltage controller step responses after the addition of the SC. The inset on the power controller step response plot also clarifies that apart from minor differences in the transient behaviour of the controller, there is no major impact on system performance. The voltage controller response shown in Figure 4 shows that the SC has made the voltage controller response slower. However, no further noticeable difference in dynamic or steady-state performance is seen to have been introduced by the SC, suggesting that an SC can enhance the system damping.

3) STRONG GRID CASE

The system is further tested on a high SCR grid (strong-grid case with SCR = 4.12). The step plots shown in 5 show that in a strongly connected WPP, the addition of an SC doesn't change the system stability and small-signal performance in any significant way.

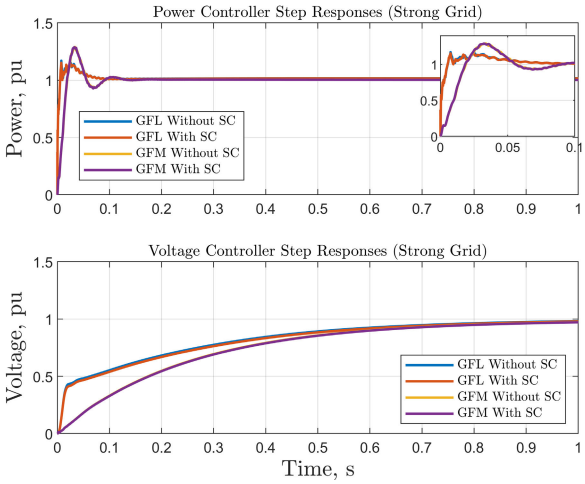

FIGURE 5. Power and voltage controller step response of GFL and GFM converters in a strongly connected WPP with and without an SC.

B. EIGENVALUE ANALYSIS

To better understand the impact of SCs on WPP stability, further analyses are presented in terms of system eigenvalues for different operating points. For each of the sub-cases in Table 1, eigenvalue analysis is performed for a range of 27 different operating points defined as grid voltage reference(V_g^*), wind turbine voltage reference (V_{turb}^*), and wind turbine power references (P_{turb}^*) as shown in Table 2.

TABLE 2. WTG operating points utilised for eigenvalue studies.

Reference	Values		
Grid Voltage Reference (V_g^*)	0.95	1.0	1.05
Turbine Voltage Reference (V_{turb}^*)	0.95	1.0	1.05
Turbine Power Reference (P_{turb}^*)	0.1	0.5	1.0

The eigenvalues of the system for the 27 operating points given in 2 are coalesced in one figure and plotted in Figure 6 for weak-grid case, Figure 7 for normal-grid case, and 8. Eigenvalue damping is also defined and marked in the eigenvalue plots with dotted lines. The eigenvalue damping is given as:

$$\zeta_i = -\frac{\Re\{\lambda_i\}}{|\lambda_i|}, \tag{44}$$

where λ_i is the i^{th} eigenvalue. Eigenvalue damping ratios marked in the plots are helpful for understanding system stability as low and near-synchronous frequency oscillations with higher than 20% damping ratio ensure well-damped oscillations during normal operating conditions.

1) WEAK GRID CASE

The poles on the right-hand side of the $s-$plane in figure 6 suggest that irrespective of GFL or GFM control, for operating points with low grid and turbine voltage references

($V^*_{turb} = 0.95$ pu, $V^*_g = 0.95$ pu), the weakly connected OF WPP exhibits small-signal instability. For the nominal operating point, the step responses in Figure 3 showed that the GFM WPP system stayed stable even without the addition of the SC. However, for other operating points, as seen from Figure 6, the system becomes unstable, and the addition of an SC at the PCC stabilises it. Near-synchronous frequency modes with poor damping (i.e. poles with $\zeta < 20\%$) are also seen in cases where turbine and grid voltage references were at their lower levels, i.e. $V^*_{turb} = 0.95$ pu, $V^*_g = 0.95$ pu.

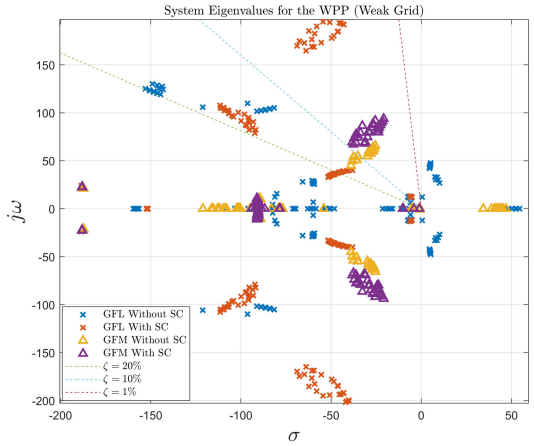

FIGURE 6. Eigenvalues for weak-grid case (27 standard operating points superimposed).

2) NORMAL GRID CASE

The normal-grid connected case for the OF WPP did not exhibit any stability issues with or without the SC across the selected 27 operating points. There are some changes in the eigenvalue location as shown in Figure 7; however, the eigenvalue damping and frequencies change only slightly, and there is no significant change in system stability. This was also observed in the step responses calculated for the nominal case in Figure 4. Further, the low-damped, near-synchronous eigenvalues from the weak-grid case are well-damped in this case. This further suggests that some unstable system modes are stabilised with SCs in a weakly connected system. At the same time, a normal-grid connection does not necessarily require SCs to enhance system stability. Furthermore, poorly damped near-synchronous oscillatory modes (not prevalent in normal grids) are not strongly affected by SCs in weak grids; grid strength plays a crucial role in the elimination/damping of near-synchronous modes than SCs do.

3) STRONG GRID CASE

Further eigenvalue analysis for a strong grid with SCR = 4.12 is performed on all the predefined operating points (see Table 2). The eigenvalue plots for this case presented in figure 8 also show that for a strongly connected OF WPP, adding an SC does not change the system poles in any discernible way.

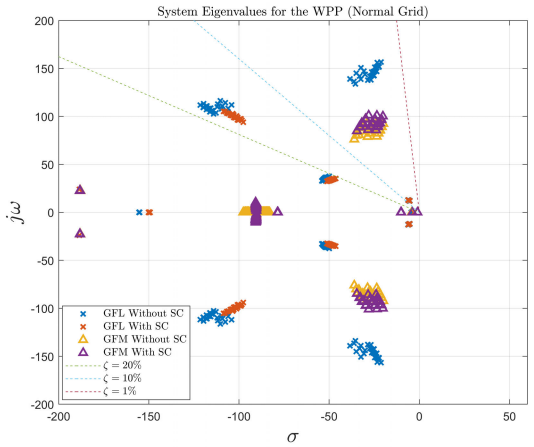

FIGURE 7. Eigenvalues for normal-grid case (27 standard operating points superimposed).

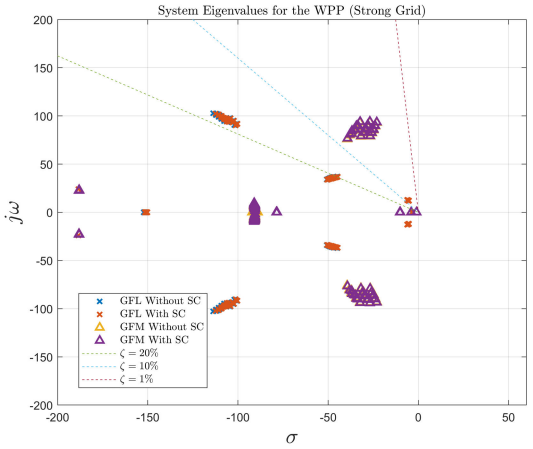

FIGURE 8. Eigenvalues for Strong-grid case (27 standard operating points superimposed).

4) LOWEST EIGENVALUE DAMPING

For the normal operating point $V^*_g = 1.0$, $V^*_{turb} = 1.0$, $P^*_{turb} = 1.0$, the following table (Table 3) summarises the most critical modes which exhibit lowest system damping.

TABLE 3. Summary of lowest damped modes (λ_{min}) and damping ratio (ζ) for the normal operating point $V^*_g = 1.0$, $V^*_{turb} = 1.0$, $P^*_{turb} = 1.0$.

WPP Control	Weak Grid	Normal Grid	Strong Grid
GFL W/O SC	7.54 ± j33.13 ζ = -22.19 %	-5.24 ± j12.13 ζ = 39.65 %	-5.73 ± j12.48 ζ = 41.72 %
GFL W SC	-5.68 ± j12.46 ζ = 41.47 %	-5.17 ± j12.03 ζ = 39.48 %	-5.66 ± j12.41 ζ = 41.49 %
GFM W/O SC	-35.13 ± j54.86 ζ = 53.92 %	-19.93 ± j92.33 ζ = 21.09 %	-32.44 ± j84.63 ζ = 35.79 %
GFM W SC	-32.67 ± j86.41 ζ = 35.36 %	-20.18 ± j100.15 ζ = 19.75 %	-31.21 ± j93.27 ζ = 31.73 %

As seen from Table 3, SC enhances the small-signal stability for a weak-grid case by increasing the lowest system damping for GFL OF WPP. However, its impact is minimal on the small-signal stability of a normal-grid-connected

and strong-grid-connected OF WPP. No significant damping improvements are seen for GFM OF WPP, suggesting that SC offers overall system damping improvement as opposed to GFM converter control. It must be noted that this table summarises the most critical modes over one standard operating point.

Further, based on the eigenvalues plotted for various operating conditions and grid strengths in Figures 6, 7, and 8, a summary of the lowest damped modes and the respective damping ration for each case is presented in Table 4 below. This table summarises the most critical modes with the least damping over the 27 operating points defined earlier in Table 2.

TABLE 4. Summary of lowest damped modes (λ_{min}) and damping ratio (ζ) for the 27 standard operating points V_g^* = [0.95 1.0 1.05], V_{turb}^* = [0.95 1.0 1.05], P_{turb}^* = [0.1 0.5 1.0].

WPP Control	Weak Grid	Normal Grid	Strong Grid
GFL W/O SC	54.54 (unstable)	-21.21 + 984.19i ζ =2.15 %	-5.17 + 76.40i ζ =6.75 %
GFL W/ SC	-5.16 + 76.59i ζ =6.72 %	-5.18 + 75.56i ζ =6.83 %	-5.17 + 76.34i ζ =6.75 %
GFM W/O SC	46.97 + 0.00i (unstable)	-19.93 + 580.12i ζ =3.43 %	-22.97 + 584.90i ζ =3.92 %
GFM W/ SC	-0.87 + 5.27i ζ =16.26 %	-20.18 + 629.26i ζ =3.20 %	-23.05 + 587.41i ζ =3.92 %

An analysis of the lowest system damping and associated critical modes over the 27 standard operating points studied in this paper shows that SC enhances the small-signal stability for a weak-grid case by increasing the lowest system damping for both GFL and GFM-controlled OF WPP. However, its impact on the small-signal stability of a strong grid is minimal. For a normal-grid-connected case, the lowest system damping could be improved for GFL OF WPP with an SC. However, no significant damping improvements are seen for GFM OF WPP, suggesting that SC offers overall system damping improvement as opposed to GFM converter control.

C. EQUIVALENT SHORT CIRCUIT RATIO

The ESCR of the system before and after the addition of the SC was calculated using the time-domain simulation models as well as based on the procedure described in III. Short-circuit levels for both these methods are presented in figure 9. The short-circuit MVA is presented in pu with the base of the WPP apparent power rating S_{WPP}. Table 5 below summarises the SCR values based on these results. In either of these cases, the contribution of converters to the effective SCR is not considered.

From 9 and Table 5, the effective SCR of the WPP is seen to have increased significantly after the introduction of the SC. This also shows a good match between the theoretical calculation and time-domain simulation-based results. Based on Figure 9 and Equation (42), the SCR enhancing properties of SCs is elaborated. Further, (42) could be utilised to estimate the enhanced short-circuit level of the WPP, including the effect of the SC. This expression not only

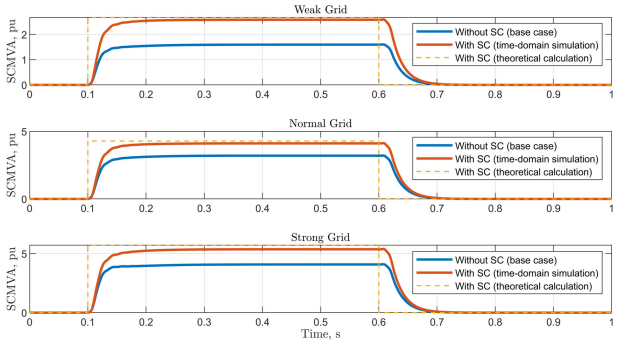

FIGURE 9. SCMVA levels based on theoretical calculation and time-domain simulations.

TABLE 5. SCR enhancement of a WPP at WT MV terminals based on theoretical calculation vs fault MVA simulations: with and SC.

Grid Case	W/O SC	W/ SC (theoretical)	W/ SC (simulation)
Weak Grid	SCR = 1.6	SCR = 2.67	SCR = 2.58
Normal Grid	SCR = 3.2	SCR = 4.28	SCR = 4.11
Strong Grid	SCR = 4.12	SCR = 5.71	SCR = 5.37

helps illustrate the SCR-enhancing properties of SC in an OF WPP but also aids in the short-circuit calculations and further assists in other power plant design considerations. However, for specific converter control methods, the effective contribution to system strength needs to be quantified and proposals on such are available in the academic literature [30]. Furthermore, since the scope of our work is related to small-signal studies and SCR calculations, for study considerations regarding converter and SC control interactions, further detailed information on the overall system stability needs to be gathered with a more detailed SC model, including its control dynamics and immittance-based stability analysis methods.

V. CONCLUSION

A small-signal and a time-domain model of the aggregated OF WPP were constructed, and the effect of the addition of an SC in such a system was studied for different cases. The analysis shows that for a weakly connected OF WPP, an SC can have a significant positive impact on stability. It can enhance the small-signal stability, improve the system response by damping out oscillations, and enhance the SCR of the system. The stabilizing effect is more significant for GFL WPPs than for GFM WPPs. For a normal-grid-connected and strongly connected OF WPP, no significant stability improvements were observed for the tested 27 operating points. However, the effective SCR of the system was seen to have been improved due to the addition of the SC in both these cases. Even though frequency domain analysis didn't show significant improvement in the small signal stability of the WPPs in these two cases, the SC can still aid in the overall fault response of the WPP and improve the dynamic stability.

With GFM control of the WTGs, stability issues were observed for fewer operating points. Further analysis seems necessary to fully understand the stability performance of SCs and GFM converters and to investigate if a GFM converter can have the same or better stability performance as a GFL converter and SC pair. However, as seen from the eigenvalue analyses and study of ESCR, it is clear that although GFM converters do not enhance system ESCR, they can still improve the system small-signal stability. Further work on re-defining ESCR for power systems with GFM converters included is needed to understand the overall impact of GFM converters on system strength. Furthermore, SCs are seen to improve both ESCR and system stability. After appropriate quantification of system ESCR with GFM converters, our work can help choose between a GFM OF-WPP and GFL OF-WPP with an SC based on small-signal stability, converter-driven stability, voltage stability, and system strength perspective.

VI. FUTURE WORKS

For any study type, model fidelity and applicability are crucial points. The studies that could be performed on a specific model are dependent on the type of models considered. For future studies, such as harmonic analyses, full switching models of the converters, the inclusion of SC control dynamics, and the full EMT model of the overall system can be utilised. Further, the future stability impact of other support devices, such as STATCOM and energy storage devices, could also be compared against both SCs and GFM OF WPPs. As HVDC-connected OF WPPs and HVDC hubs such as energy islands and multi-terminal HVDC projects are being studied in Europe and other parts of the world, SCs and GFM converters can both be invaluable for localised stability improvement, reactive power support, and inertial support. Thus, for MMC-based HVDC converters used in such projects, small-signal stability studies are not sufficient. Thus, further time-domain dynamic studies based on full-order EMT models and detailed harmonic studies will be crucial. Considering this, further research could include the study of overall stability enhancement (small-signal stability, harmonic stability, transient stability, and voltage stability) via synchronous condensers and GFM converters.

LEGAL DISCLAIMER

This work was supported by Innovation Fund Denmark under the project Ref. no. 0153-00256B. Figures and values presented in this paper should not be used to judge the performance of Siemens Gamesa Renewable Energy technology as they are solely presented for demonstration purposes. Any opinions or analyses contained in this paper are the opinions of the authors and are not necessarily the same as those of Siemens Gamesa Renewable Energy.

CONFLICT OF INTEREST

The authors declare no conflict of interest.

APPENDIX A
TEST SYSTEM PARAMETERS

The system parameters used in this paper are summarised below in Table 6.

TABLE 6. System parameters used in the simulation studies. All parameters are in pu unless otherwise stated.

Parameter	Notation	Value
SC impedance	$Z_{sc,pu}$	j0.14
SC transformer impedance	$Z_{tr,pu}$	0.0016+j0.08
Array transformer impedance	$Z_{tf,pu}$	0.0008+j0.004
Filter parameters	Z_f	0.0063+j0.0265
Filter capacitance	C_f	5×10^{-6}
PLL PI gains	$K_p^{(pll)}$, $K_i^{(pll)}$	0.025, 1.5
PLL Bandwidth	$\Delta\omega_{PLL}$	7.5 Hz
Virtual inertia	J	1
Damping constant	D_p	50
PC Bandwidth	$\Delta\omega_{pc}$	50 Hz
Reactive power droop	K_q	0.2
GFM VC PI gains	$K_p^{(vc)}$, $K_i^{(vc)}$	0.05, 0.039
GFM CC P-gain	$K_p^{(cc)}$, $K_i^{(cc)}$	10.5, 16
GFL CC PI gains	$K_p^{(cc)}$, $K_i^{(cc)}$	0.05, 0.30
GFL CC Bandwidth	$\Delta\omega_{cc}$	150 Hz
PWM Delay	T_{pwm}	0.19 ms
Sampling Time	T_s	0.2 ms
SC rating	S_{sc}	$0.5S_{WPP}$
System base power	S_{base}	S_{WPP}

APPENDIX B
PARTICIPATION FACTOR ANALYSIS FOR THE UNSTABLE POLE PAIR

A participation factor analysis is performed for a pair of unstable poles in one of the study cases (Weak Grid GFL W/O SC, $V_g^* = 1.0\ pu$, $V_{turb}^* = 1.0\ pu$, $P_{turb}^* = 1.0\ pu$) and is presented in Table 7 below.

The participation factor analysis for the unstable mode (pole pair) shows that the current and voltage controller states participate in unstable modes. Although this indicates the stability problem as a controller-driven stability problem, some participating states are also related to the cable states and shall not be overlooked. Current and voltage controller states are current and voltage measurements after filtering, and the cable states are cable currents and voltages. Thus, although a preliminary participation factor analysis shows the

TABLE 7. Participation factor analysis of the unstable mode ($f = 4.63\ Hz$, $\zeta = -22.27$) in the unstable case (Weak Grid GFL W/O SC, $V_g^* = 1.0\ pu$, $V_{turb}^* = 1.0\ pu$, $P_{turb}^* = 1.0\ pu$).

S.No.	State Name	Participation Factor
1	CCtrlState1	20.26 %
2	VCtrlState1	11.67 %
3	CCtrlState2	11.47 %
4	PLLState2	10.66 %
5	VCtrlState2	7.67 %
6	PLLState2	4.48 %
7	VCtrlState3	2.58 %
8	VCtrlState4	2.34 %
9	CableState1	2.33 %
10	CableState2	2.29 %

impact of the faster inner control loops on the system stability, it must be noted that the impacting states are dependent on cable states. Thus, the instability issue could be solved either as a control or as a system issue. Our results also support this statement as the inclusion of a synchronous condenser in the OF WPP solved the issue for GFL control case, as well as the use of a GFM converter instead of a GFL converter solved the issue; however, this depends on the grid strength. For reference, Figures 3, 4, and 5, and Table 3 can be useful.

APPENDIX C
PQ DIAGRAMS

Figure 10 shows the reactive power delivery by a GFL OF WPP (from Figure 1) for different active power set-points at various grid SCR values. The figure suggests that for a strong-grid connected case indicated by high SCR, the OF WPP needs to supply minimal reactive power to facilitate the power flow. However, for a weak-grid connected case, depending on the active power set-point, the OF WPP needs to supply larger reactive power to facilitate the power flow.

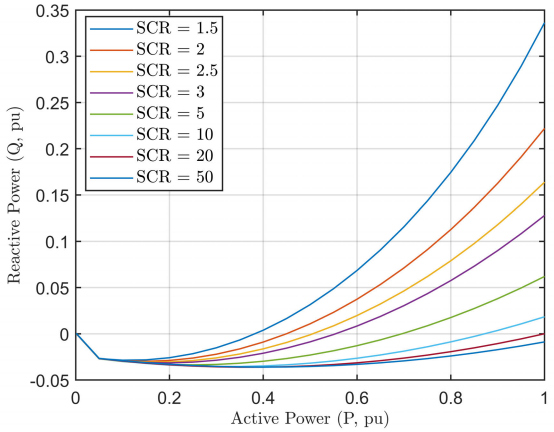

FIGURE 10. PQ relationship diagram for an offshore WPP connected to a power grid of different grid strength.

REFERENCES

[1] *Connection of Wind Farms to Weak AC Networks*, document CIGRE Study Committee WG B4.62, Working Group on Wind Farm Connection, Tech. Brochures, 2016.
[2] L. Fan and Z. Miao, "An explanation of oscillations due to wind power plants weak grid interconnection," *IEEE Trans. Sustain. Energy*, vol. 9, no. 1, pp. 488–490, Jan. 2018.
[3] P. S. Kundur, N. J. Balu, and M. G. Lauby, "Power system dynamics and stability," *Power Syst. Stability Control*, vol. 3, pp. 700–701, Dec. 2017.
[4] W. Li, Z. Qian, Q. Wang, Y. Wang, F. Liu, L. Zhu, and S. Cheng, "Transient voltage control of sending-end wind farm using a synchronous condenser under commutation failure of HVDC transmission system," *IEEE Access*, vol. 9, pp. 54900–54911, 2021.
[5] Y. Katsuya, Y. Mitani, and K. Tsuji, "Power system stabilization by synchronous condenser with fast excitation control," in *Proc. PowerCon. Int. Conf. Power Syst. Technol.*, vol. 3, 2000, pp. 1563–1568.
[6] *Pathways Towards A Robust Future Energy System*, Energinet, Erritsø, Denmark, 2023.
[7] *Summary: Security of Electricity Supply*, Energinet, Erritsø, Denmark, 2017.
[8] *Ancillary Services From New Technologies*, Energinet, Erritsø, Denmark, Dec. 2019.
[9] *Executive Summary: Stet0043*, Energinet, Erritsø, Denmark, 2023.
[10] S.-H. Huang, J. Schmall, J. Conto, J. Adams, Y. Zhang, and C. Carter, "Voltage control challenges on weak grids with high penetration of wind generation: Ercot experience," in *Proc. IEEE Power Energy Soc. Gen. Meeting*, Jul. 2012, pp. 1–7.
[11] P. E. Marken, M. Henderson, D. LaForest, J. Skliutas, J. Roedel, and T. Campbell, "Selection of synchronous condenser technology for the granite substation," in *Proc. IEEE PES T&D*, Apr. 2010, pp. 1–6.
[12] H. T. Nguyen, G. Yang, A. H. Nielsen, and P. H. Jensen, "Combination of synchronous condenser and synthetic inertia for frequency stability enhancement in low-inertia systems," *IEEE Trans. Sustain. Energy*, vol. 10, no. 3, pp. 997–1005, Jul. 2019.
[13] H. Zhang, J.-P. Hasler, N. Johansson, L. Ängquist, and H.-P. Nee, "Frequency response improvement with synchronous condenser and power electronics converters," in *Proc. IEEE 3rd Int. Future Energy Electron. Conf. ECCE Asia (IFEEC-ECCE Asia)*, Jun. 2017, pp. 1002–1007.
[14] H. T. Nguyen, C. Guerriero, G. Yang, C. J. Boltonand, T. Rahman, and P. H. Jensen, "Talega synCon—Power grid support for renewable-based systems," in *Proc. SoutheastCon*, Apr. 2019, pp. 1–6.
[15] L. Bao, L. Fan, and Z. Miao, "Comparison of synchronous condenser and STATCOM for wind farms in weak grids," in *Proc. 52nd North Amer. Power Symp. (NAPS)*, Apr. 2021, pp. 1–6.
[16] D. Pattabiraman, R. H. Lasseter, and T. M. Jahns, "Comparison of grid following and grid forming control for a high inverter penetration power system," in *Proc. IEEE Power Energy Soc. Gen. Meeting (PESGM)*, Aug. 2018, pp. 1–5.
[17] K. V. Kkuni, M. Nuhic, and G. Yang, "Power system stability impact assessment for the current limits of grid supporting voltage-source converters," in *Proc. IEEE Power Energy Soc. Gen. Meeting (PESGM)*, Jul. 2021, pp. 1–5.
[18] M. Nuhic and G. Yang, "A hybrid system consisting of synchronous condenser and battery—Enhanced services for weak systems," in *Proc. IEEE PES Innov. Smart Grid Technol. Eur. (ISGT-Europe)*, Sep. 2019, pp. 1–5.
[19] J. Jia, G. Yang, A. H. Nielsen, and P. Rønne-Hansen, "Impact of VSC control strategies and incorporation of synchronous condensers on distance protection under unbalanced faults," *IEEE Trans. Ind. Electron.*, vol. 66, no. 2, pp. 1108–1118, Feb. 2019.
[20] J. Jia, G. Yang, A. H. Nielsen, E. Muljadi, P. Weinreich-Jensen, and V. Gevorgian, "Synchronous condenser allocation for improving system short circuit ratio," in *Proc. 5th Int. Conf. Electr. Power Energy Convers. Syst. (EPECS)*, Apr. 2018, pp. 1–5.
[21] L. Richard, T. K. Saha, W. Tushar, and H. Gu, "Optimal allocation of synchronous condensers in wind dominated power grids," *IEEE Access*, vol. 8, pp. 45400–45410, 2020.
[22] Y. Wang, L. Wang, and Q. Jiang, "Impact of synchronous condenser on sub/super-synchronous oscillations in wind farms," *IEEE Trans. Power Del.*, vol. 36, no. 4, pp. 2075–2084, Aug. 2021.
[23] V. A. Lacerda, E. P. Araujo, M. Cheah-Mañe, and O. Gomis-Bellmunt, "Phasor modeling approaches and simulation guidelines of voltage-source converters in grid-integration studies," *IEEE Access*, vol. 10, pp. 51826–51838, 2022.
[24] H. Saadat, *Power System Analysis*. Arlington, VA, USA: PSA Publishing LLC, 2010.
[25] T. J. E. Miller, *Reactive Power Control in Electric Systems*. Hoboken, NJ, USA: Wiley, 1982.
[26] *Technical Issues Related to New Transmission Lines in Denmark*, Energinet, Erritsø, Denmark, 2023.
[27] S. Ghosh, M. K. Bakhshizadeh, G. Yang, and L. Kocewiak, "An improved nonlinear stability assessment methodology for type-4 wind turbines via time reversal trajectory," 2023, *arXiv:2307.11445*.
[28] S. Ghimire, K. V. Kkuni, S. C. Jakobsen, T. Knueppel, K. H. Jensen, E. Guest, T. W. Rasmussen, and G. Yang, "Grid-forming control methods for weakly connected offshore WPPs," in *Proc. 22nd Wind Sol. Integr. Workshop (WIW)*, 2023, pp. 246–253.
[29] *IEEE Guide for Planning DC Links Terminating at AC Locations Having Low Short-Circuit Capacities*, Standard 1204–1997, 1997, pp. 1–216.
[30] C. Henderson, A. Egea-Alvarez, T. Kneuppel, G. Yang, and L. Xu, "Grid strength impedance metric: An alternative to SCR for evaluating system strength in converter dominated systems," *IEEE Trans. Power Del.*, vol. 39, no. 1, pp. 386–396, Feb. 2024.

SULAV GHIMIRE (Graduate Student Member, IEEE) received the bachelor's degree in electrical engineering from the Institute of Engineering, Tribhuvan University, Lalitpur, Nepal, in 2018, and the M.Sc. degree in energy systems from the Skolkovo Institute of Science and Technology, Moscow, Russia, in 2021. He is currently an Innovation Fund Denmark-funded joint Industrial Ph.D. Student at Siemens Gamesa Renewable Energy (SGRE) and the Technical University of Denmark (DTU) under project reference number 0153-00256B. He was an Assistant Lecturer with United Technical College, Pokhara University, Chitwan, Nepal, in 2019. From 2017 to 2019, he was the Founding Director of Karnika Innovations Pvt. Ltd. His research interests include power converter modeling, control optimization, and stability studies for offshore wind power plant applications.

KANAKESH VATTA KKUNI (Member, IEEE) received the master's degree in electrical engineering from Indian Institute of Technology Bombay, in 2014, and the Ph.D. degree from the Technical University of Denmark (DTU), in 2022. From 2014 to 2016, he was a Research Engineer with the Energy Management and Microgrid Laboratory, National University of Singapore (NUS). From 2016 to 2018, he was a Research Engineer at Berkeley Education Alliance for Research in Singapore. He is currently a Power Systems Engineer with Siemens Gamesa Renewable Energy A/S. His research interests include power system stability, power converter EMT, and real-time modeling and control.

EMERSON D. GUEST received the bachelor's degree in electrical engineering from The University of Newcastle, Newcastle, Australia, in 2010, the M.Sc. degree in electrical engineering from the Technical University of Denmark, Kongens Lyngby, Denmark, in 2014, and the joint Industrial Ph.D. degree in electrical engineering from Siemens Gamesa Renewable Energy A/S, Brande, Denmark, and the Technical University of Denmark, in 2019. He is currently a Power Systems Engineer with Siemens Gamesa Renewable Energy A/S. His research interests include harmonic modeling and small-signal stability of grid-connected converters, active filtering, and adaptive control.

KIM H. JENSEN received the M.Sc. and Ph.D. degrees from the Technical University of Denmark, Kongens Lyngby, Denmark, in 1999 and 2003, respectively. He was with Transmission Company (NESA), Consultant Company (Elsam Engineering), and currently with Siemens Gamesa Renewable Energy A/S, Kongens Lyngby. During his career, he has worked with transmission system planning, network designs, wind turbine modeling, grid code studies, harmonic analysis, and stability studies. He has also worked as a Technical Specialist on a number of wind power plant integration projects.

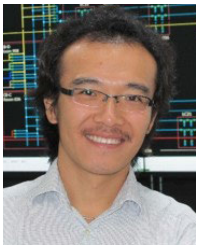

GUANGYA YANG (Senior Member, IEEE) received the Ph.D. degree from The University of Queensland, Australia, in 2008. He joined the Technical University of Denmark. From 2020 to 2021, he was a Specialist in electrical design, control, and protection of large offshore wind farms with Ørsted. He is currently an Associate Professor with the Technical University of Denmark. His current research interests include the stability and protection of converter-based power systems, with an emphasis on offshore wind applications. He is the Convener of IEC61400-21-5 on configuration, functional specification, and validation of hardware-in-the-loop test bench for wind power plants. In addition, he is the Coordinator of the H2020 Marie Curie Innovative Training Network Project "InnoCyPES (Innovative Tools for Cyber-Physical Energy Systems)" and the Lead Editor of the Power and Energy Society Section in IEEE Access.